Fracture properties of thermally modified spruce wood (Picea abies) at different moisture contents

Miran Merhar, Rostand Moutou Pitti, Tom Argensse

▶ **To cite this version:**

Miran Merhar, Rostand Moutou Pitti, Tom Argensse. Fracture properties of thermally modified spruce wood (Picea abies) at different moisture contents. Wood Material Science and Engineering, 2023, 18 (6), pp.2093-2103. 10.1080/17480272.2023.2228280 . hal-04364390

HAL Id: hal-04364390
https://hal.science/hal-04364390

Submitted on 28 Dec 2023

HAL is a multi-disciplinary open access archive for the deposit and dissemination of scientific research documents, whether they are published or not. The documents may come from teaching and research institutions in France or abroad, or from public or private research centers.

L'archive ouverte pluridisciplinaire **HAL**, est destinée au dépôt et à la diffusion de documents scientifiques de niveau recherche, publiés ou non, émanant des établissements d'enseignement et de recherche français ou étrangers, des laboratoires publics ou privés.

Fracture properties of thermally modified spruce wood (*Picea abies*) at different moisture contents

Miran Merhar[a], Rostand Moutou Pitti[b], Tom Argensse[b]

[a]University of Ljubljana, Biotechnical Faculty, Department of Wood Science and Technology, 1000 Ljubljana, Slovenia

[b]Université Clermont Auvergne, Clermont Auvergne INP, CNRS, Institut Pascal, F-63000 CLERMONTFERRAND, France

CONTACT: Miran Merhar, Miran.Merhar@bf.uni-lj.si

Abstract

The effects of different levels of thermal modification of spruce wood on the fracture properties of wood exposed to different moisture contents was investigated. Specimens were thermally modified at temperatures of 180 °C, 200 °C and 230 °C and then equilibrated together with unmodified specimens at relative humidities of 20 %, 44 %, 76 % and 88 %. Double cantilever beam specimens with TL and RL orientation were used for testing. The crack length was determined by digital image correlation and the compliance of the specimen was determined by multiple unloading of the specimen. The strain energy release rate was calculated, which decreased with increasing degree of modification and increased with increasing moisture content. The analysis showed that the strain energy release rate increased more with moisture content for unmodified samples, while the dependence of the release rate on moisture wasn't so clear for modified samples. The strain energy release rate values are higher in the TL orientation than in the RL orientation, while the crack length has no significant influence. The highest strain energy release rate was 0.256 N/mm for the unmodified TL specimens exposed to 88 % relative humidity and the lowest was 0.071 N/mm for the RL orientation of the thermally modified specimens at 220 °C and then exposed to 88 % relative humidity. From all measurements, functions were fitted to calculate the strain energy release rate as a function of orientation, degree of modification, moisture content and density of the spruce wood, which can be used to calculate the strain energy release rate for any combination of the factors studied.

Keywords: double cantilever beam, strain energy release rate, compliance, fracture process zone

Introduction

The use of wood for building purposes is increasing every year, as wood offers a sustainable building principle. Currently, coniferous wood is still mainly used, but the use of hardwood is also increasing, with spruce making up a large proportion of softwood in Europe. However, as wood is biodegradable and subject to decomposition by rot fungi, especially in high humidity, it needs to be protected. In the past, mainly chemical preservatives were used, but they're very controversial from an environmental point of view because they endanger health.

Thermal modification of wood is a more environmentally friendly way to protect against pests, but thermal modification also changes the properties of the wood. Positive changes include increased dimensional stability and reduced hygroscopicity, as well as increased bio-resistance (Bekhta and Niemz 2003, Tjeerdsma *et al.* 1998). However, the degree of thermal modification usually also reduces the mechanical properties, which is undesirable. Thus, various authors have found a decrease in density, elastic modulus and strength in different directions for different tree species of thermally

modified wood (Andor and Lagaňa 2018, Kurul and Görgün 2022, Molinski *et al.* 2018, Nhacila *et al.* 2020, Roszyk *et al.* 2020, Wang *et al.* 2018). In addition to thermal modifications, various types of modifications are also known which also affect the mechanical and other wood properties (Thybring and Fredriksson 2021).

In addition to elastic and strength properties, thermal modification also alters fracture properties. The change in fracture properties of thermally modified wood has been studied by several authors (Hlásková *et al.* 2021, Hughes *et al.* 2015, Majano-Majano *et al.* 2012, Murata *et al.* 2013, Pitti *et al.* 2016, Sebera *et al.* 2019), mostly investigating various modification levels at one wood moisture content, or one modification level at different moisture contents of the wood (Hanincová *et al.* 2022, Reiterer and Tschegg 2002, Stanzl-Tschegg and Navi 2009, Stanzl-Tschegg *et al.* 1995, Tukiainen and Hughes 2016, Vasic and Stanzl-Tschegg 2007, Xavier, Monteiro*, et al.* 2014).

One of the first to study fracture properties based on the stress intensity factor of rectilinearly anisotropic material was Sih (Sih *et al.* 1965). Shortly after Rice (1968) developed the well-known J-integral based on the stress and strain energy around the crack tip. Today, the contributions of both authors form the basis for various recent approaches to determine the fracture toughness of wood (El Kabir *et al.* 2018, Moutou Pitti *et al.* 2008, Odounga *et al.* 2018, Subramanyam Reddy *et al.* 2018), which in turn can give different results using different approaches (Merhar *et al.* 2013).

Various specimen shapes are known for fracture characterization (Kumar 2009), where only the initial crack length and the maximum force at which the crack begins to propagate need to be known. The disadvantage of this method is that only the initiating fracture property of the wood can be determined, which may change over the course of the sample due to the variability of the wood. Thus, the length of the crack can have a significant influence, especially in shorter samples where the proportion of the length of the fracture process zone to the total crack length in the wood is much greater than in samples with longer cracks (Stanzl-Tschegg and Navi 2009, Stanzl-Tschegg *et al.* 1995). However, a much better insight into the fracture behavior is obtained if the crack length is measured at the same time as the force measurement, because in this case the fracture behavior can be calculated over the entire crack. One such specimen shape that enables stable crack progression is certainly the double cantilever beam (DCB), where the length of the crack can be monitored by digital image correlation. The latter combination is very common in recent research (Gómez-Royuela *et al.* 2022, Moutou Pitti *et al.* 2014, Oliveira *et al.* 2021, Yu *et al.* 2021, Zanganeh *et al.* 2013). An alternative to the determination of the crack length is also by the compliance of the sample, from which the equivalent crack length can be calculated (Crespo *et al.* 2018, El Moustaphaoui *et al.* 2021, Pečnik *et al.* 2022, Xavier, Oliveira*, et al.* 2014).

The aim of the study is therefore to investigate the overall influence of different factors on the fracture properties of spruce wood, both for different levels of thermal modification, different wood moisture contents and for the direction of tissue loading, with the crack progressing in the longitudinal direction. Furthermore, the influence of the crack length on the fracture properties is also investigated. Based on the results, functions for calculating the fracture properties of spruce wood for all the above factors, including wood density, are developed.

Materials and methods

Specimen preparation

A 4 m long spruce *(Picea abies*) board with a cross-section of 350 mm x 55 mm and constant growth ring width was first cut into 4 pieces of 1 m length. One piece was left unmodified (A group), and the other three were thermally modified using the Silvapro process (Rep *et al.* 2012). The first piece was treated at 180 °C (B group), the second at 200 °C (C group) and the third at 230 °C (D group), where the mass loses were 1.8 %, 4% and 10.6 % respectively. After modification, all pieces were stored at 22°C and 65% relative humidity for six months to allow internal stresses to relax.

Each single piece of 1 m length was then cut into 4 smaller pieces of 245 mm length, from which 10 samples of 245 mm x 22 mm x 22 mm were cut. The individual groups of 10 samples were then equilibrated to a constant sample mass at 22 °C and relative humidity (RH) of 20 %, 44 %, 76 %, and 88 %. After final equilibration of the samples, their exact dimensions and mass were measured and the density for each sample was determined. The specimens were then cut to a final size of 200 mm x 20 mm x 20 mm. The double cantilever beam (DCB) was used for testing. 5 specimens were used for TL orientation (force action in tangential direction with crack propagation in longitudinal direction) and 5 for RL (force action in radial direction with crack propagation in longitudinal direction) orientation. Additional specimens were used to determine the equilibrium moisture content (EMC) of the wood for each combination of moisture content and thermal modification. They were weighed after equilibrium adjustment, then dried at 103 °C to absolute dryness and weighed again to determine moisture content.

From end of the specimen, an 85 mm cut was first made with a band saw, followed by a cca 1 mm cut with a sharp knife. Holes 3 mm in diameter were also drilled in the specimens for clamping, as shown in Figure 1. The final effective length of the notch from the clamping point was thus about 79 mm, and the exact length was measured on each specimen after the test was completed.

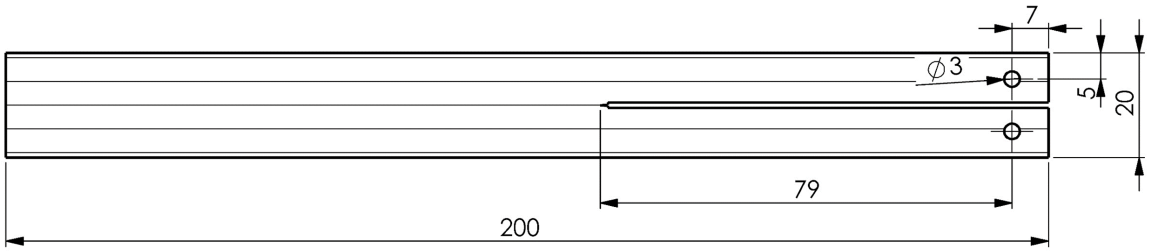

Figure 1. Double cantilever beam (DCB) specimen

On the side where crack propagation was observed, the specimens were painted with white acrylic paint. First, one coat was applied. After drying, the surface was sanded with 500 grit sandpaper and a second coat was applied. After the white paint dried, the black paint was sprayed on to create a speckled pattern. After the paint dried, two more parallel lines were drawn at 60 mm distance, which served as distance calibration for the subsequent determination of the crack length using the Digital Image Corelation (DIC) method. The samples prepared in this way were then put again into the climatic chambers with the above-mentioned relative humidities in order to re-equilibrate them to a constant mass.

After final conditioning, the specimens were clamped in the universal testing machine, as shown in Figure 2. The specimens were loaded at a feed rate of 6 mm/min. The magnitude of the force was recorded at a sampling rate of 100 Hz, and the crack path was recorded with a Huawei P30 ELE-L29 camera at a distance of 10 cm from the specimen. Since two parallel lines were drawn at a distance of 60 mm for calibration at each specimen, the exact distance of the camera from the specimen was not important. Before the experiment, a grid of horizontal and vertical lines was also created to check if

the image was distorted. Since this was not the case, the camera met our requirements. The images with a resolution of 3840 x 2160 dpi were taken every 5 seconds.

After an initial crack advance of a few millimetres, the machine was stopped and the camera took 1-2 pictures in 6 seconds. The specimens were then unloaded at a rate of 25 mm/min by 60% of the deflection and then reloaded at the same rate up to the deflection before unloading. From this point, the test was continued at a feed rate of 6 mm/min. When the crack had again advanced by about 10 mm, the entire procedure was repeated, so that 5 to 6 measurements were taken on each specimen.

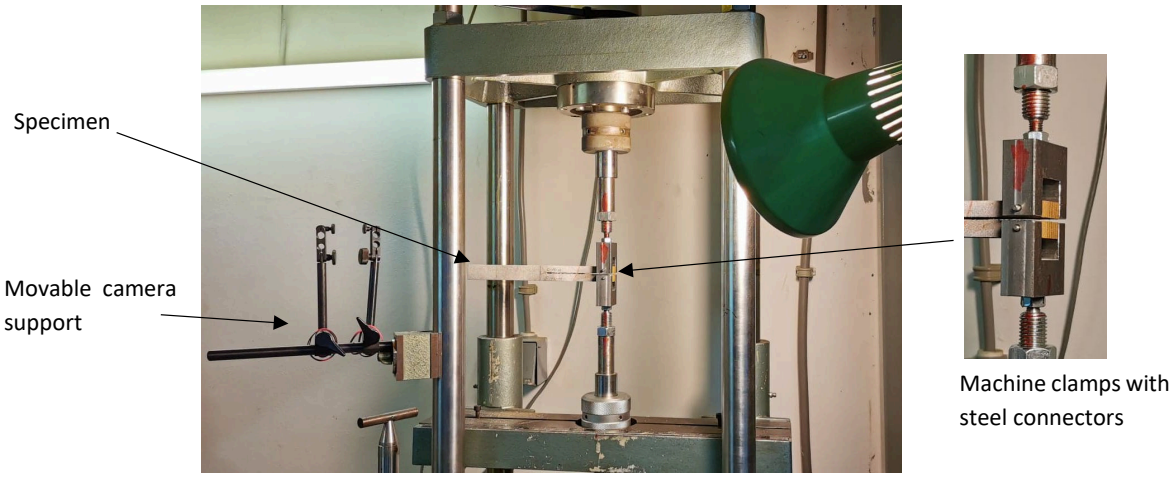

Figure 2. Experimental system

The resulting measurements were then used to determine the crack length and the corresponding compliance of the specimen at the specified crack lengths. The crack length was determined using the DIC programme GOM Correlate. A facet size of 10 pixels and a point spacing of 5 pixels were used to create the surface components. A scale of 32 pixels/mm was defined by vertical lines spaced 60 mm apart. The calculation of the specific deformation in the y-direction was performed using the images. Although the images showed the visible length of the crack, the strain at the visible crack tip was 10 % or more, which is well above the failure strain of 0.62 % and 0.33 % for the tangential and radial directions, respectively, considering the transverse modulus of elasticity in the tangential and radial directions of 420 MPa and 770 MPa, respectively (Ross 2010) and the transverse tensile strength of 2.6 MPa. The position of the crack tip was thus determined from the stress in front of the crack tip. The critical stress intensity factor was taken from the literature (Stanzl-Tschegg *et al.* 1995), which is for spruce on average 0.55 MPa$\sqrt{\mathrm{m}}$ and 0.6 MPa$\sqrt{\mathrm{m}}$ for TL and RL orientations, respectively. The stress at a distance of 1 mm in front of the crack tip was calculated using the equation (Kumar 2009, Smith *et al.* 2003), at the angle θ=0°

$$\sigma_{22R} = \frac{K_I}{\sqrt{2\,\pi\,r}}\cos\frac{\theta}{2}\left(1+\sin\frac{\theta}{2}\sin\frac{3\theta}{2}\right) = \frac{0.6\ \mathrm{MPa}\sqrt{\mathrm{m}}}{\sqrt{2\,\pi\,0.001\mathrm{m}}} = 7.56\ \mathrm{MPa}$$
$$\sigma_{22T} = \frac{K_I}{\sqrt{2\,\pi\,r}}\cos\frac{\theta}{2}\left(1+\sin\frac{\theta}{2}\sin\frac{3\theta}{2}\right) = \frac{0.55\ \mathrm{MPa}\sqrt{\mathrm{m}}}{\sqrt{2\,\pi\,0.001\mathrm{m}}} = 6.94\ \mathrm{MPa} \quad (1)$$

where K_I is critical stress intensity factor in mode I, θ is angle and r is distance at the direction of interest.

Taking into account the modulus of elasticity in the radial and tangential directions of 770 MPa and 420 MPa, respectively (Ross 2010), the specific deformation (strain) at a distance of 1 mm is.

$$\varepsilon_{yR} = \frac{\sigma_{22R}}{E_R} = \frac{7.56\ \text{MPa}}{770\ \text{MPa}} = 0.98\% \qquad (2)$$
$$\varepsilon_{yT} = \frac{\sigma_{22T}}{E_T} = \frac{6.94\ \text{MPa}}{420\ \text{MPa}} = 1.6\%$$

At the visible crack tip, the specific deformation in the y-direction was read off the course line from the DIC analysis. The location with a specific deformation of 0.98 % and 1.6 % in the y-direction for the RL and TL orientations was located and then the distance between this location and the visible crack tip was determined. The total length of the crack was therefore the sum of the initial notch created by the band saw, the length of the visible crack and the length between the visible crack tip and the location with the above-mentioned strain in the y-direction minus 1 mm. The distance between the visible crack tip and the tip of the actual crack can be attributed to the fracture process zone FPZ (Crespo *et al.* 2018), which includes a toughening mechanism such as microcracking and fibre bridging.

As will be seen from the results, the distance between the location of the 0.98 % strain and the 1.6 % strain is less than a tenth of a millimetre, so the method described was used with the 1.6 % strain value for all humidities and modification levels. The critical stress intensity factor and modulus of elasticity vary with both humidity and different levels of modification, but the error was estimated to be small, especially compared to the variability within and between specimens.

From the values thus obtained for crack length, force and compliance, the strain energy release rate was calculated using the equation (Dourado *et al.* 2010, Kumar 2009)

$$G_I = \frac{3P^2C}{2ab} \qquad (3)$$

Where G_I is the strain energy release rate for mode I, b is the specimen width and P and C are the force and compliance at crack length a, respectively.

Using the resulting strain energy release values for the different combinations, a univariate linear regression test was performed using Statgraphics software to determine the significant influence of each factor, and a fit function was determined.

Results and discussion

Figure 3 shows the crack length analysis for an unmodified TL orientation sample conditioned at 10 % relative air humidity together with force and crack mouth opening displacement measurement showing on figure 4. The upper part of the figure 3 shows the advanced visible crack length of 25.2 mm and the lower part of the figure shows the strain in the y-direction. From the figure it can be seen that the strain at the end of the visible part of the crack is 10.86 %. This means that with a transverse modulus of elasticity of 420 MPa in the tangential direction (Ross 2010) and a tensile strength of 2.6 MPa, there is a cracked area, but it is not visible to the naked eye due to the micro-failure in the fracture process zone.

Starting from the visible crack tip in the crack propagation direction, Figure 5 shows strain in the y-direction with value of 1.6 % is at a distance of 1.5 mm from the visible crack tip. Since the strain was

calculated to be 1.6 % at a distance of 1 mm from the actual crack tip (Equation 1 and 2), this means that the total length of the advancing crack is 25.2mm +1.5 mm -1 mm = 25.7 mm. If the initial notch length of 79 mm is added, the total length of the crack is 104.7 mm.

The strain of 0.98 % is at a distance of 1.55 mm (Figure 5), which is only 0.05 mm more than a distance with a strain of 1.6 %. Since a difference in distance of 0.05 mm represents only an error of 0.05 % for a crack length of 100 mm and even less for a longer crack, the length at a strain of 1.6 % was used in the rest of analyses to determine the crack length. The method described proved to be suitable, especially if one takes into account the coefficient of variation, which ranges from 10 % to 24 %, as will be presented later.

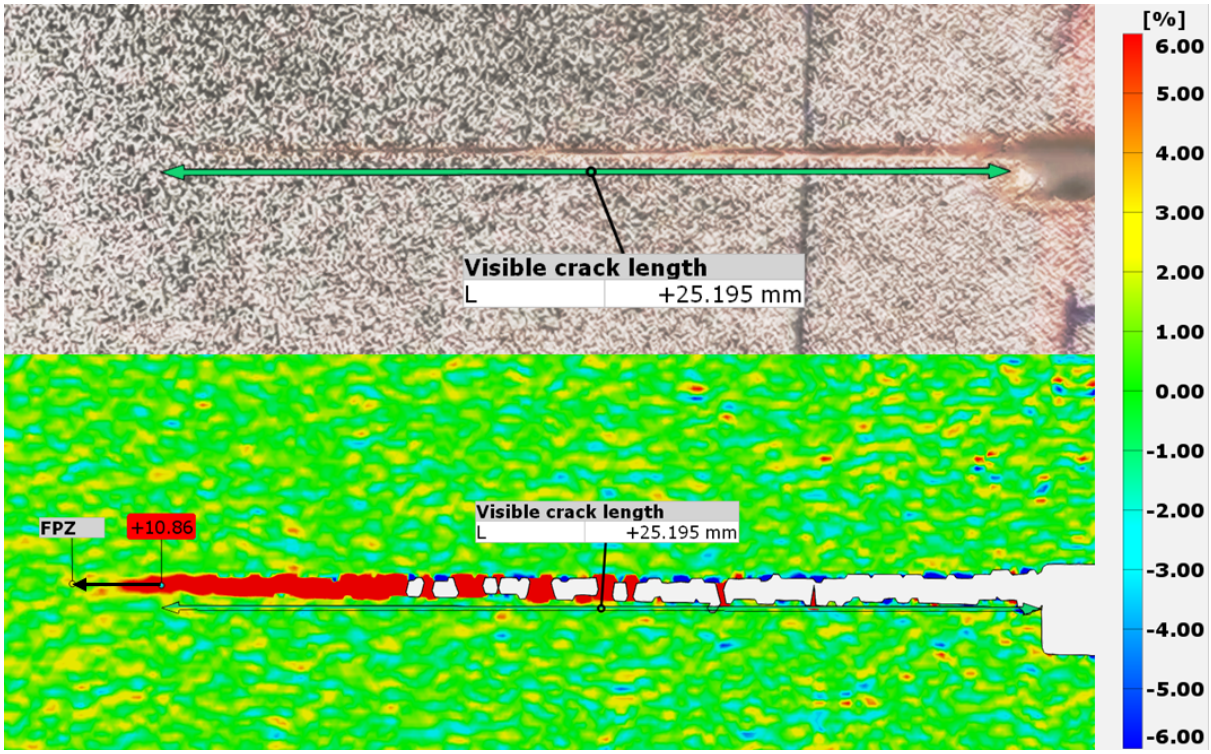

Figure 3. Visible crack (upper) and strain distribution in y direction

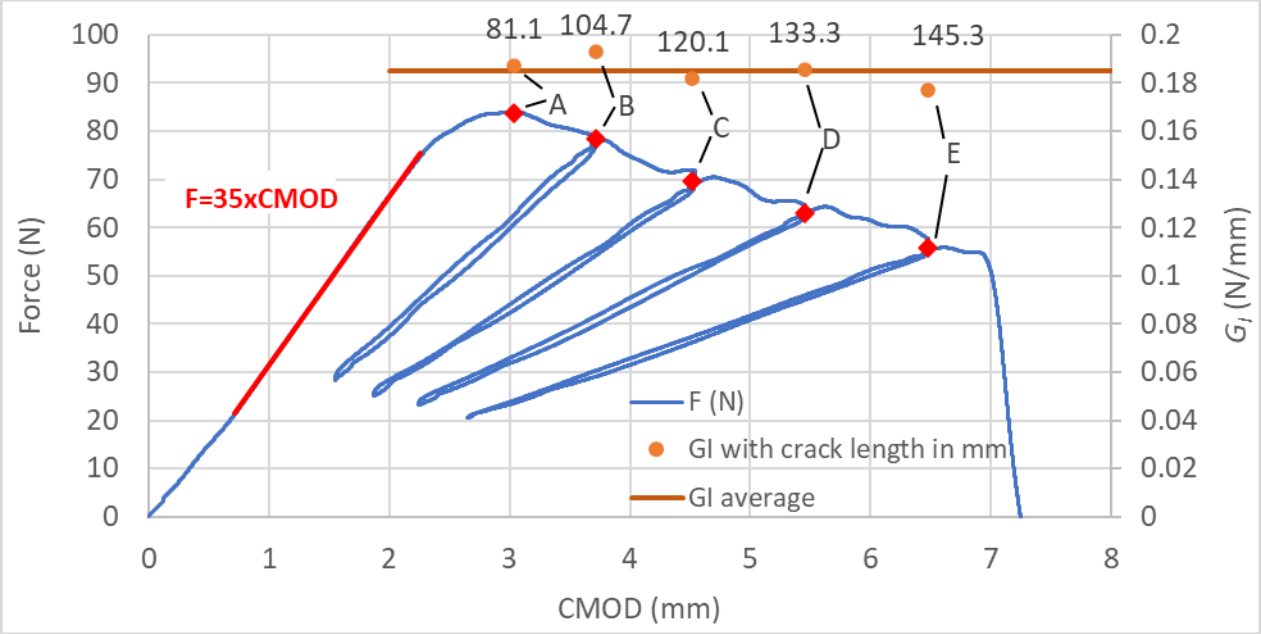

Figure 4. Force and crack mouth displacement measurement, together with strain energy release rates and corresponding crack lengths (in mm)

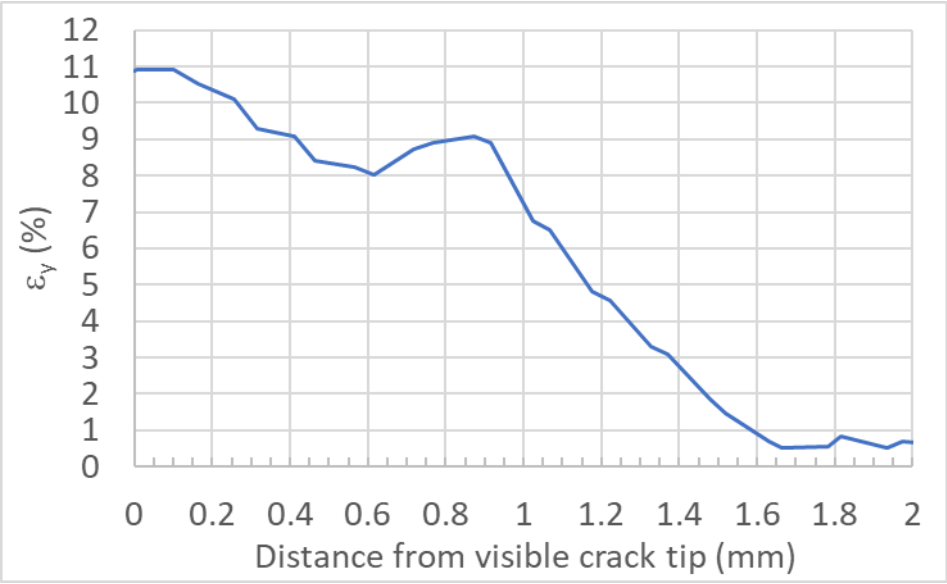

Figure 5. Strain in y direction in front of the crack tip in the direction of crack propagation

The first the part of the force crack mouth displacement curve (Figure 4) is slightly non-linear, as the specimen is still adjusting to the clamping, then the linear part corresponding to the compliance of the specimen with the initial crack length (81.1 mm), and then again, the non-linear part when the fracture process zone is established (Xavier, Oliveira*, et al.* 2014). After the maximum force, the crack starts to progress. The maximum force at point A, the initial crack length of 81.1 mm and the compliance from the first linear part (F=35x CMOD) give the first G_I value of 0.187 N/mm. The further the crack progresses, the lower the force becomes. After the crack had progressed for a certain distance, the machine was stopped (point B), the force was determined, an image was taken for DIC analysis and then the compliance of the specimen was determined from the part of the curve below

point B. The same was done for points C to E. For the points A to E there are also given corresponding crack lengths for which strain energy release rates were calculated. The graph shows that the value of G_I slightly varies with crack length by the average value of 0.185 N/mm, but there is no distinctive influence of the crack length on the values of strain energy release rates.

The strain energy release rate values and the trend lines for the TL and RL orientations of all measured values as a function of the crack length, the relative air humidity and the degree of modifications are shown in Figure 6 where the strain energy release rate either increases or decreases with crack length, while decreases with the degree of thermal modification. This trend is more pronounced in the unmodified specimens than in the modified specimens. To determine the effect of crack length on the strain energy release rate, a univariate regression test for main effects was performed. The results in Table 1 show that crack length has no significant effect on strain energy release rate at significant level p=0.05. Although the samples were made from a single board with a more or less uniform growth ring width, the samples from the same group had quite different densities. The univariate regression test for main effects confirmed a significant influence of density. The moisture content as well as the degree of modification also have a significant influence on the strain energy release rate.

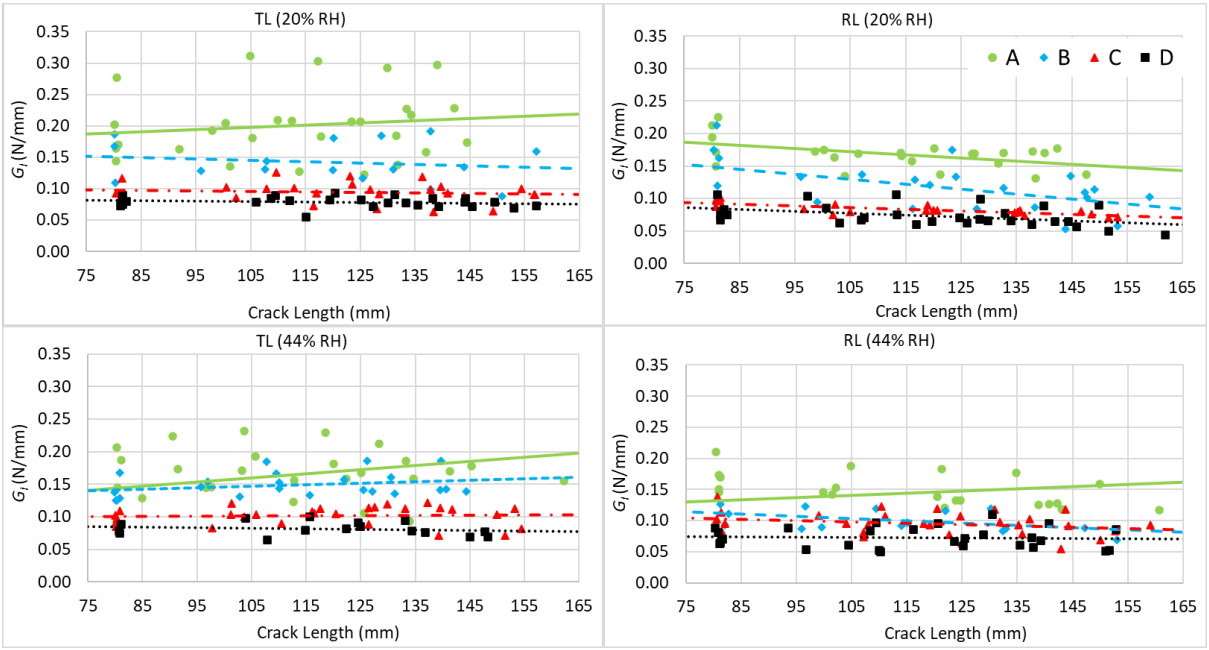

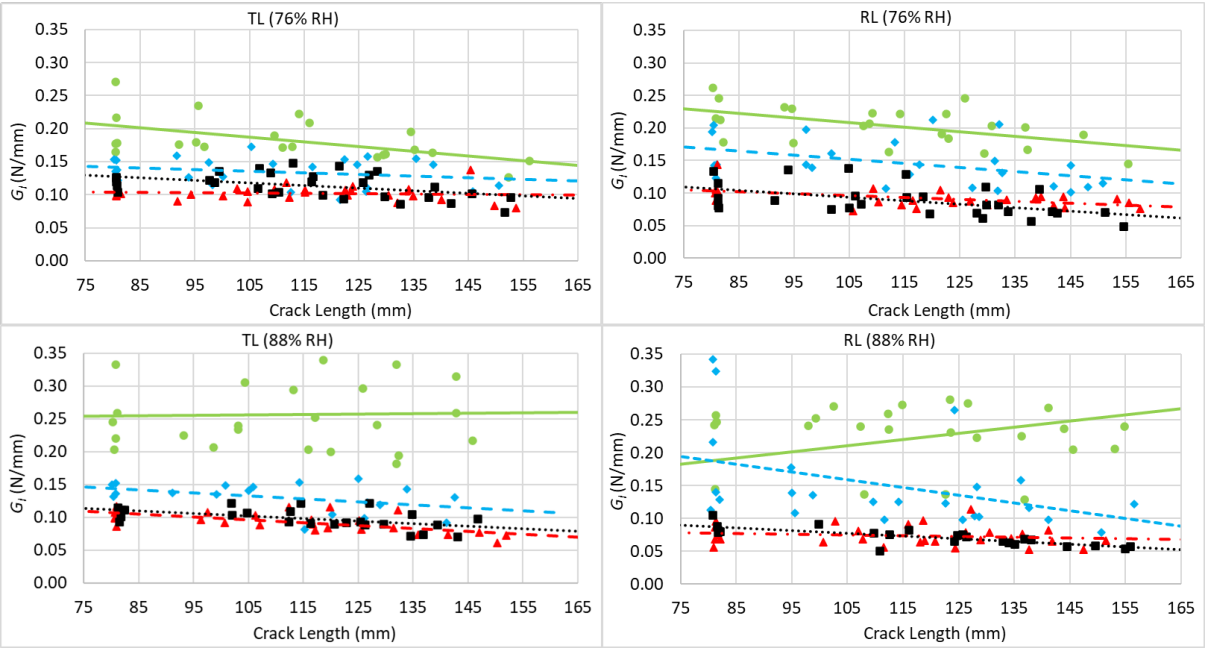

Figure 6. Strain energy release rates for all measured values at different crack lengths, unmodified (A) and modified samples (180 °C (B), 200 °C (C) and 230 °C (D)), at different relative air humidities (RH) and orientations (TL and RL)

Table 1. Univariate linear regression test for main effects at significant level p=0.05

Crack length	Density	Relative humidity	Modification	Orientation
0.956	0.000	0.000	0.035	0.000

The average values of strain energy release rates for the different conditions, together with the standard deviations, average densities and moisture contents of the samples at different relative air humidities are shown in Figure 7 and Table 2. It can be seen that the equilibrium moisture contents of the wood at the same relative air humidity decreases with the degree of thermal modification, which is consistent with the literature (Bekhta and Niemz 2003). The average values of strain energy release rate of the unmodified samples for the RL and TL orientations at the lowest relative humidity of 20% are 0.143 N/mm and 0.201 N/mm, respectively, which then increase to 0.227 N/mm and 0.256 N/mm at the highest humidity of 88%, which is also in agreement with the literature (Majano-Majano *et al.* 2012, Stanzl-Tschegg and Navi 2009, Vasic and Stanzl-Tschegg 2007, Xavier, Monteiro*, et al.* 2014). The lower values in the RL orientation can be attributed to the fact that the crack propagates through the earlywood, which has a lower strain energy release rate than the latewood (Xavier, Monteiro*, et al.* 2014), while in the TL configuration the crack propagates through both earlywood and latewood simultaneously.

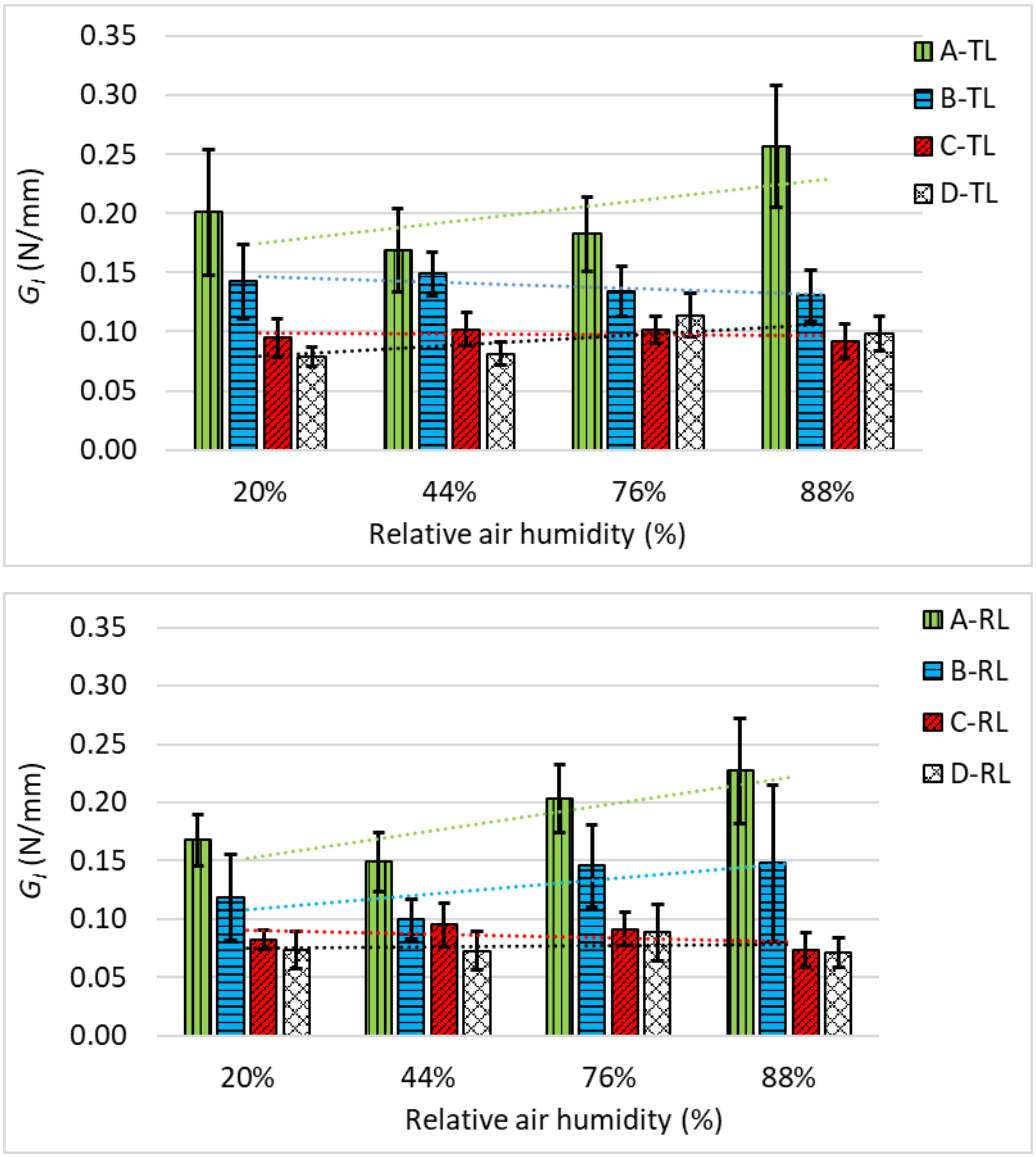

Figure 7. Average values of strain energy release rates (G_I), standard deviations of strain energy release rates (vertical lines) at different degrees of thermal modifications (A, B, C, D), orientations of the samples (TL, RL) and various relative air humidities

Table 2. Values of equilibrium moisture content (*EMC*) of samples, strain energy release rates (G_I), standard deviations of strain energy release rates (*SD* G_I), coefficient of variation of strain energy release rate (*COV* G_I) as a function of relative humidity (*RH*), degree of thermal modification (A, B, C, D) and orientation of the sample (TL, RL) together with average specimen density (ρ) and standard deviation of specimen density (*SD* ρ).

	RH (%)	*EMC* (%)	G_I (N/mm)	SD G_I (N/mm)	COV G_I (%)	ρ (kg/m^3)	*SD* ρ (kg/m^3)
A-TL	20	7.2	0.201	0.053	26.4	479	30
	44	9.9	0.169	0.035	20.9	477	34
	76	13.3	0.182	0.031	17.1	472	29
	88	19.1	0.256	0.052	20.1	499	28

B-TL	20	5	0.143	0.031	22.0	464	52
	44	6.6	0.149	0.018	12.3	445	26
	76	10.7	0.134	0.021	15.8	461	28
	88	16.2	0.131	0.022	16.6	472	42
C-TL	20	4	0.095	0.016	16.8	445	23
	44	5.7	0.102	0.014	13.7	451	25
	76	8.8	0.102	0.011	10.9	459	26
	88	11.8	0.092	0.015	16.4	443	94
D-TL	20	3.8	0.079	0.008	10.1	438	24
	44	5.7	0.081	0.010	12.4	424	25
	76	8.5	0.114	0.018	16.1	468	7
	88	10.5	0.098	0.015	14.8	451	21
A-RL	20	7.2	0.168	0.022	13.0	476	36
	44	9.9	0.149	0.025	17.0	476	32
	76	13.3	0.203	0.030	14.6	482	33
	88	19.1	0.227	0.045	19.8	482	38
B-RL	20	5	0.119	0.037	31.3	448	16
	44	6.6	0.100	0.017	16.9	445	30
	76	10.7	0.146	0.035	23.9	432	20
	88	16.2	0.148	0.067	45.2	436	17
C-RL	20	4	0.083	0.008	9.9	444	34
	44	5.7	0.095	0.018	19.5	452	25
	76	8.8	0.092	0.014	15.4	462	31
	88	11.8	0.073	0.015	20.4	460	30
D-RL	20	3.8	0.073	0.016	21.7	436	31
	44	5.7	0.073	0.016	22.5	423	22
	76	8.5	0.088	0.024	27.0	450	18
	88	10.5	0.071	0.013	18.0	432	26

While the trend of increasing strain energy release rate with humidity is clear for unmodified specimens for both TL and RL orientations, the trend is not so pronounced for thermally modified specimens. Thus, the trend is decreasing for thermal modification B and TL orientation, while it is increasing for RL orientation. For thermal modifications C and D (200 and 230 °C), the increasing and decreasing trends are not so clear. Thus, for the C samples, the increasing/decreasing trend is not clear for the TL orientation, while it slightly decreases for the RL orientation. For the D samples, the trend is slightly increasing for the TL orientation, but again not clear for the RL orientation. The trend of an increasing strain energy release rate with the moisture content of thermally modified wood was also noted by Majano-Majano (2012).

Figure 8 shows the quadratic fitting functions for strain energy release rate as a function of density and relative air humidity for all test combinations, while Table 3 shows the corresponding equations together with the correlation coefficient. Linear functions were also fitted but had significantly lower correlation coefficients. The functions are useful for calculating strain energy release rates, but only over the range of values used in the test. Since the unmodified samples had a density of 410 to 540 kg/m^3, the function is only useful in this density range, while the relative humidity for all samples was between 20% and 88%. However, as the degree of modification increases, the densities decrease and

so does the range of application of the functions for modified spruce wood. It is also evident from the figures that the functions decrease or increase very rapidly outside the tested range, so that their applicability outside the tested range is questionable.

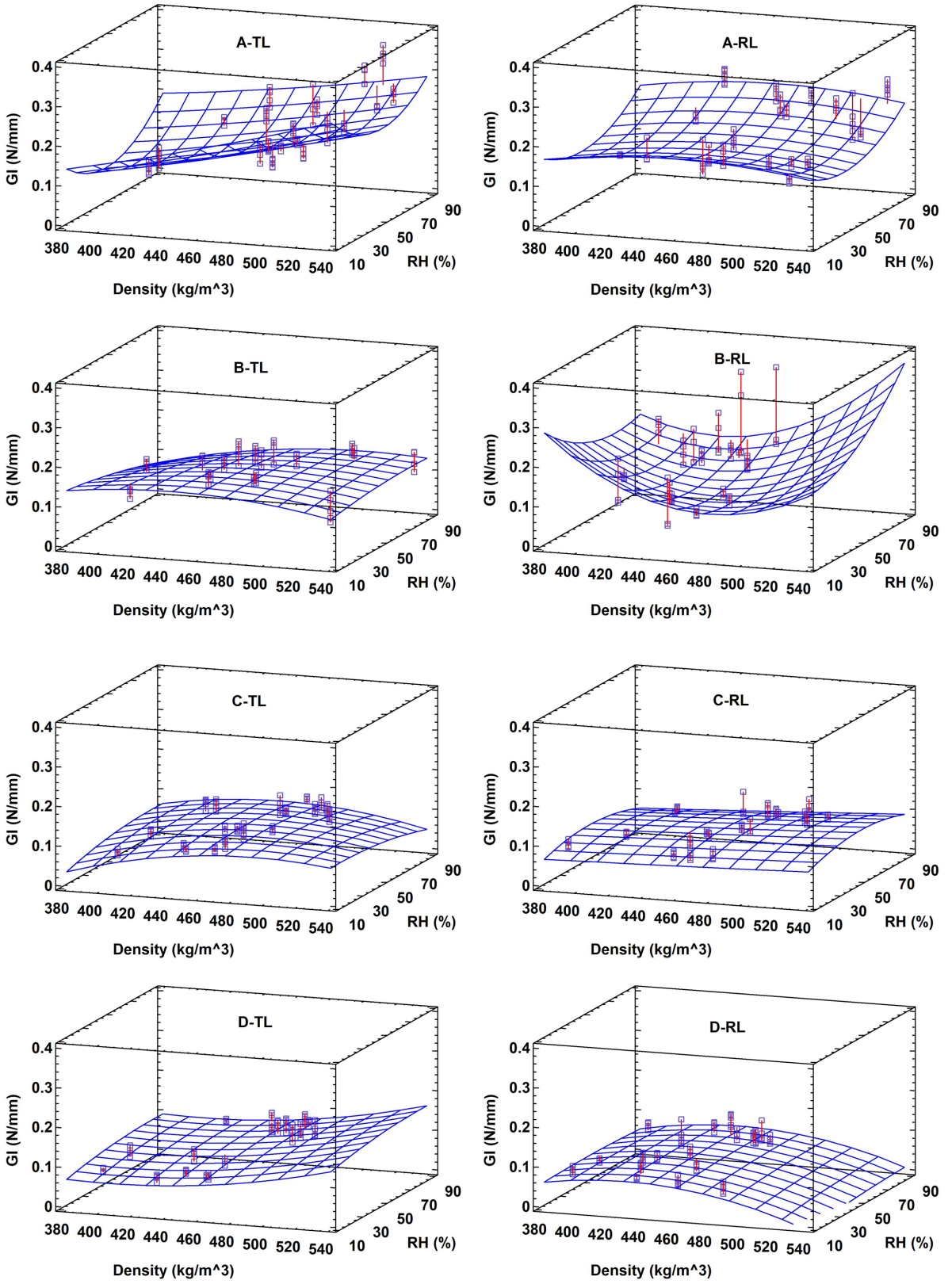

Figure 8 Fitted surface function

Table 3 Fitted functions of strain energy release rate *G* (N/mm) in dependence of density (kg/m^3) and relative air humidity RH (%) and R-squared

Condition	Equation	R^2
A-TL	$G_I = 0.00301129 + 0.00000196336 * Density - 0.00195255 * RH + 0.00000119209 * Density^2 - 0.00000580778 * Density * RH + 0.0000484495 * RH^2$	0.51
A-RL	$G_I = -0.673062 + 0.00388573 * Density - 0.00309552 * RH - 0.00000424764 * Density^2 + 5.71888E-7 * Density * RH + 0.0000350826 * RH^2$	0.48
B-TL	$G_I = -0.673522 + 0.00380579 * Density - 0.00276632 * RH - 0.00000436787 * Density^2 + 0.00000642955 * Density * RH - 0.00000478902 * RH^2$	0.21
B-RL	$G_I = 4.26132 - 0.0170209 * Density - 0.0125977 * RH + 0.0000175022 * Density^2 + 0.0000226258 * Density * RH + 0.0000288291 * RH^2$	0.21
C-TL	$G_I = -1.29467 + 0.00559696 * Density + 0.00340415 * RH - 0.00000561871 * Density^2 - 0.00000580861 * Density * RH - 0.00000752044 * RH^2$	0.44
C-RL	$G_I = 0.0358999 - 0.00000660036 * Density + 0.00106364 * RH + 1.13685E-7 * Density^2 + 0.0000012838 * Density * RH - 0.0000164469 * RH^2$	0.32
D-TL	$G_I = 0.704238 - 0.00319919 * Density + 0.000835611 * RH + 0.00000394294 * Density^2 + 1.33395E-7 * Density * RH - 0.00000533775 * RH^2$	0.45
D-RL	$G_I = -1.23888 + 0.00614571 * Density - 0.000550159 * RH - 0.00000719653 * Density^2 + 0.00000199951 * Density * RH - 0.00000235732 * RH^2$	0.13

Conclusions

In the study, a comprehensive analysis of the effects of the degree of thermal modification of spruce wood exposed to different moisture contents and sample orientations on the fracture properties was carried out. From the investigations carried out, it can be concluded:

- The strain energy release rate decreases with increasing the degree of modification.

- The strain energy release rate increases with increasing moisture content of the wood. This trend is most evident with unmodified wood, while it's no longer evident at modified specimens. Thus, at higher degrees of modification, it can be positive or even negative.

- The strain energy release rate was independent of the crack length in the tested samples

- The length of the fracture zone was negligible and didn't have a major influence on the strain energy release rate

- The strain energy release rate increases with specimen density.

- Based on the degree of thermal modification, wood moisture content, orientation and wood density, a function was fitted to calculate the strain energy release rate as a function of these factors

The results obtained show that the critical strain energy release rate depends, among other things, on the moisture content and the density of the wood species depending on the direction of crack propagation. In future work, mixed-mode cracking will be performed in order to assess which cracking mode is the most discriminating in the degradation process of these thermally modified materials. In

addition, a numerical finite element model will also be implemented to anticipate the complex loading modes compared to the tests that will be performed.

Funding: The research was supported by the Programs P2-0182, co-financed by the Slovenian Research Agency.

Conflicts of Interest: The authors declare no conflict of interest.

ORCID

Miran Merhar https://orcid.org/0000-0003-0420-787X

Rostand Moutou Pitti https://orcid.org/0000-0002-4596-4693

References

Andor, T. and Lagaňa, R. (2018). Selected properties of thermally treated ash wood. *Acta Facultatis Xylologiae, 60*(1), 51-60. doi:10.17423/afx.2018.60.1.06

Bekhta, P. and Niemz, P. (2003). Effect of high temperature on the change in color, dimensional stability and mechanical properties of spruce wood. *Holzforschung, 57*(5), 539-546. doi:10.1515/HF.2003.080

Crespo, J., Majano-Majano, A., Xavier, J. and Guaita, M. (2018). Determination of the resistance-curve in Eucalyptus globulus through double cantilever beam tests. *Materials and Structures/Materiaux et Constructions, 51*(3). doi:10.1617/s11527-018-1209-9

Dourado, N. M. M., De Moura, M. F. S. F., Morais, J. J. L. and Silva, M. A. L. (2010). Estimate of resistance-curve in wood through the double cantilever beam test. *Holzforschung, 64*(1), 119-126. doi:10.1515/HF.2010.010

El Kabir, S., Dubois, F., Moutou Pitti, R., Recho, N. and Lapusta, Y. (2018). A new analytical generalization of the J and G-theta integrals for planar cracks in a three-dimensional medium. *Theoretical and Applied Fracture Mechanics, 94*, 101-109. doi:10.1016/j.tafmec.2018.01.004

El Moustaphaoui, A., Chouaf, A., Kimakh, K. and Chergui, M. (2021). Determination of the onset and propagation criteria of delamination of Ceiba plywood by an experimental and numerical analysis. *Wood Material Science and Engineering, 16*(5), 325-335. doi:10.1080/17480272.2020.1737963

Gómez-Royuela, J. L., Majano-Majano, A., Lara-Bocanegra, A. J., Xavier, J. and de Moura, M. F. S. F. (2022). Evaluation of R-curves and cohesive law in mode I of European beech. *Theoretical and Applied Fracture Mechanics, 118*. doi:10.1016/j.tafmec.2021.103220

Hanincová, L., Procházka, J., Novák, V. and Kopecký, Z. (2022). Influence of Moisture Content on Cutting Parameters and Fracture Characteristics of Spruce and Oak Wood. *Drvna Industrija, 73*(3), 341-349. doi:10.5552/DRVIND.2022.0026

Hlásková, L., Procházka, J., Novák, V., Čermák, P. and Kopecký, Z. (2021). Interaction between thermal modification temperature of spruce wood and the cutting and fracture parameters. *Materials, 14*(20). doi:10.3390/ma14206218

Hughes, M., Hill, C. and Pfriem, A. (2015). The toughness of hygrothermally modified wood: COST Action FP0904 2010-2014: Thermo-hydro-mechanical wood behavior and processing. *Holzforschung, 69*(7), 851-862. doi:10.1515/hf-2014-0184

Kumar, P. (2009). *Elements Of Fracture Mechanics*. New Delhi [etc.]: Tata McGraw-Hill.

Kurul, F. and Görgün, H. V. (2022). EFFECT OF THERMAL MODIFICATION ON SOME PHYSICAL AND MECHANICAL PROPERTIES OF YELLOW POPLAR (Liriodendron tulipifera). *Drewno, 65*(209). doi:10.12841/wood.1644-3985.380.01

Majano-Majano, A., Hughes, M. and Fernandez-Cabo, J. L. (2012). The fracture toughness and properties of thermally modified beech and ash at different moisture contents. *Wood Science and Technology, 46*(1-3), 5-21. doi:10.1007/s00226-010-0389-4

Merhar, M., Bucar, D. G. and Bucar, B. (2013). Mode I Critical Stress Intensity Factor of Beech Wood (Fagus Sylvatica) in a TL Configuration: A Comparison of Different Methods. *Drvna Industrija, 64*(3), 221-229. doi:10.5552/drind.2013.1253

Molinski, W., Roszyk, E., Jablonski, A., Puszynski, J. and Cegiela, J. (2018). Mechanical parameters of thermally modified ash wood determined on compression in tangential direction. *Maderas: Ciencia y Tecnologia, 20*(2), 267-276. doi:10.4067/S0718-221X2018005021001

Moutou Pitti, R., Badulescu, C. and Grédiac, M. (2014). Characterization of a cracked specimen with full-field measurements: Direct determination of the crack tip and energy release rate calculation. *International Journal of Fracture, 187*(1), 109-121. doi:10.1007/s10704-013-9921-5

Moutou Pitti, R., Dubois, F., Petit, C., Sauvat, N. and Pop, O. (2008). A new M-integral parameter for mixed-mode crack growth in orthotropic viscoelastic material. *Engineering Fracture Mechanics, 75*(15), 4450-4465. doi:10.1016/j.engfracmech.2008.04.021

Murata, K., Watanabe, Y. and Nakano, T. (2013). Effect of Thermal Treatment on Fracture Properties and Adsorption Properties of Spruce Wood. *Materials, 6*(9), 4186-4197. doi:10.3390/ma6094186

Nhacila, F., Sitoe, E., Uetimane, E., Manhica, A., Egas, A. and Möttönen, V. (2020). Effects of thermal modification on physical and mechanical properties of Mozambican Brachystegia spiciformis and Julbernardia globiflora wood. *European Journal of Wood and Wood Products, 78*(5), 871-878. doi:10.1007/s00107-020-01576-z

Odounga, B., Moutou Pitti, R., Toussaint, E. and Grédiac, M. (2018). Mode I fracture of tropical woods using grid method. *Theoretical and Applied Fracture Mechanics, 95*, 1-17. doi:10.1016/j.tafmec.2018.02.006

Oliveira, J., Xavier, J., Pereira, F., Morais, J. and De Moura, M. (2021). Direct evaluation of mixed mode i+ii cohesive laws of wood by coupling mmb test with dic. *Materials, 14*(2), 1-12. doi:10.3390/ma14020374

Pečnik, J. G., Pondelak, A., Burnard, M. D. and Sebera, V. (2022). Mode I fracture of beech-adhesive bondline at three different temperatures. *Wood Material Science and Engineering*. doi:10.1080/17480272.2022.2135135

Pitti, R. M., Hamdi, S. E., Dubois, F., Fournely, E. and Kuzman, M. K. (2016). *Thermo-hydro fracture and viscoelastic behavior of timber based materials: Numerical analysis.* Paper presented at the WCTE 2016 - World Conference on Timber Engineering.

Reiterer, A. and Tschegg, S. (2002). The influence of moisture content on the mode I fracture behaviour of sprucewood. *Journal of Materials Science, 37*(20), 4487-4491. doi:10.1023/A:1020610231862

Rep, G., Pohleven, F. and Kosmerl, S. (2012). *Development of the industrial kiln for thermal wood modification by a procedure with an initial vacuum and commercialisation of modified Silvapro wood.* Paper presented at the the 6th European Conference on Wood Modification, Ljubljana, Slovenia.

Rice, J. R. (1968). A path independent integral and the approximate analysis of strain concentration by notches and cracks. *Journal of Applied Mechanics, Transactions ASME, 35*(2), 379-388. doi:10.1115/1.3601206

Ross, R. J. (2010). *Wood handbook : wood as an engineering material*. Madison (WI): The Forest Products Laboratory : Forest Products Society,.

Roszyk, E., Stachowska, E., Majka, J., Mania, P. and Broda, M. (2020). Moisture-dependent strength properties of thermally-modified Fraxinus excelsior wood in compression. *Materials, 13*(7), 1-12. doi:10.3390/ma13071647

Sebera, V., Redón-Santafé, M., Brabec, M., Děcký, D., Čermák, P., Tippner, J. and Milch, J. (2019). Thermally modified (TM) beech wood: Compression properties, fracture toughness and cohesive law in mode II obtained from the three-point end-notched flexure (3ENF) test. *Holzforschung, 73*(7), 663-672. doi:10.1515/hf-2018-0188

Sih, G. C., Paris, P. C. and Irwin, G. R. (1965). On cracks in rectilinearly anisotropic bodies. *International Journal of Fracture Mechanics, 1*(3), 189-203. doi:10.1007/BF00186854

Smith, I., Landis, E. and Gong, M. (2003). *Fatigue and fracture of wood*. New York ; Chichester: Wiley.

Stanzl-Tschegg, S. E. and Navi, P. (2009). Fracture behaviour of wood and its composites. A review. COST Action E35 2004-2008: Wood machining - Micromechanics and fracture. *Holzforschung, 63*(2), 139-149. doi:10.1515/HF.2009.012

Stanzl-Tschegg, S. E., Tan, D. M. and Tschegg, E. K. (1995). New splitting method for wood fracture characterization. *Wood Science and Technology, 29*(1), 31-50. doi:10.1007/BF00196930

Subramanyam Reddy, M., Ramesh, K. and Thiyagarajan, A. (2018). Evaluation of mode-I SIF, T-stress and J-integral using displacement data from digital image correlation – Revisited. *Theoretical and Applied Fracture Mechanics, 96*, 146-159. doi:10.1016/j.tafmec.2018.04.006

Thybring, E. E. and Fredriksson, M. (2021). Wood modification as a tool to understand moisture in wood. *Forests, 12*(3). doi:10.3390/f12030372

Tjeerdsma, B. F., Boonstra, M., Pizzi, A., Tekely, P. and Militz, H. (1998). Characterisation of thermally modified wood: Molecular reasons for wood performance improvement. *Holz als Roh - und Werkstoff, 56*(3), 149-153. doi:10.1007/s001070050287

Tukiainen, P. and Hughes, M. (2016). The effect of temperature and moisture content on the fracture behaviour of spruce and birch. *Holzforschung, 70*(4), 369-376. doi:10.1515/hf-2015-0017

Vasic, S. and Stanzl-Tschegg, S. (2007). Experimental and numerical investigation of wood fracture mechanisms at different humidity levels. *Holzforschung, 61*(4), 367-374. doi:10.1515/HF.2007.056

Wang, X., Chen, X., Xie, X., Wu, Y., Zhao, L., Li, Y. and Wang, S. (2018). Effects of thermal modification on the physical, chemical and micromechanical properties of Masson pine wood (Pinus massoniana Lamb.). *Holzforschung, 72*(12), 1063-1070. doi:10.1515/hf-2017-0205

Xavier, J., Monteiro, P., Morais, J. J. L., Dourado, N. and De Moura, M. F. S. F. (2014). Moisture content effect on the fracture characterisation of Pinus pinaster under mode i. *Journal of Materials Science, 49*(21), 7371-7381. doi:10.1007/s10853-014-8375-0

Xavier, J., Oliveira, M., Monteiro, P., Morais, J. J. L. and de Moura, M. F. S. F. (2014). Direct Evaluation of Cohesive Law in Mode I of Pinus pinaster by Digital Image Correlation. *Experimental Mechanics, 54*(5), 829-840. doi:10.1007/s11340-013-9838-y

Yu, Y., Xin, R., Zeng, W. and Liu, W. (2021). Fracture resistance curves of wood in the longitudinal direction using digital image correlation technique. *Theoretical and Applied Fracture Mechanics, 114*. doi:10.1016/j.tafmec.2021.102997

Zanganeh, M., Lopez-Crespo, P., Tai, Y. H. and Yates, J. R. (2013). Locating the crack tip using displacement field data: A comparative study. *Strain, 49*(2), 102-115. doi:10.1111/str.12017